Scripta Materialia 182 (2020) 43–47

Contents lists available at ScienceDirect

Scripta Materialia

journal homepage: www.elsevier.com/locate/scriptamat

Whisker growth under a controlled driving force: Pressure induced whisker nucleation and growth

Piyush Jagtap*, Nupur Jain, Eric Chason

School of Engineering, Brown University, Providence, RI, 02912, USA

ARTICLE INFO

Article history:
Received 30 January 2020
Accepted 21 February 2020
Available online 5 March 2020

Keywords:
Pressure induced whisker
Driving force
Nucleation and growth kinetics
Sn whisker

ABSTRACT

We investigate whisker nucleation and growth kinetics in Sn coatings induced by the application of mechanical pressure. The pressure was applied to the samples using a clamping fixture that enables a constant pressure to be maintained over long duration of time. The fixture is small enough so that it could be transferred inside a Scanning Electron Microscope (SEM) chamber to observe the stress driven whisker nucleation and growth in real-time while the applied pressure is maintained on the Sn films.

Whisker growth is observed from the surface of thin films or coatings of many low melting point metals and alloys (Cd, Zn, Sn, Ag, Al etc.) [1]. Many studies focusing on whisker formation have been performed on Sn and Sn-alloy coatings deposited on Cu substrates due to its widespread use in the electronics industry. In the past, the addition of a small quantity of Pb in Sn was used to prevent whisker growth [2]. However, the worldwide initiative for environmentally friendly Pb-free electronics manufacturing has eliminated this practice making whisker growth phenomenon once again an active area of research. Despite decades of research on the whisker formation phenomenon, the mechanism of whisker growth remains elusive. Although multiple whisker growth mechanisms have been proposed [3–12], there is no universally accepted explanation.

Whisker formation in Sn coatings has been proposed to be a stress relaxation phenomenon [13–16] wherein a compressive stress drives the mass transport of atoms [13]. Whiskers are, therefore, proposed to grow as long as the driving force of a stress gradient is maintained. There are many potential sources of stress in the Sn layer that can lead to whisker formation. These are deposition-induced residual stress [17], phase formation due to an interfacial reaction between Sn and an underlayer [12,14–16,18], formation of Sn-oxide on the free surface [19–21], thermal stress due to mismatch between the coefficients of thermal expansion for the Sn layer and the substrate [22–26], or the application of mechanical force [13,27–36]. In many applications that use Sn coatings on Cu-containing substrates, the diffusion-controlled reaction between Sn and Cu leads to continuous formation of Cu_6Sn_5 intermetallic compound (IMC) resulting in compressive stress in the layer [14–16,18–19,37]. However, studying this process is difficult because the stress induced by intermetallic growth is difficult to control and predict.

In order to develop a more fundamental understanding of whisker formation, it is useful to perform experiments wherein whisker growth can be studied under a controlled driving force. Pei et al. [22] developed a technique wherein the Sn thin films deposited on Si substrate were heated to impose a thermal mismatch strain and hence stress in the Sn layer. The resulting stress in the Sn layer and nuclei density was measured simultaneously in real-time by a laser curvature technique and optical microscopy, respectively. The resulting nucleation and growth kinetics could then be correlated directly with the stress [22–24]. However, the compressive stress in the Sn induced by heating to a fixed temperature (i.e., under constant thermal strain) relaxes due to power-law creep [22–23,38] making it is impossible to maintain a constant elevated stress state.

Experiments performed by Fischer et al. (1954) [13] demonstrated that compressive stress in Sn produced by the application of mechanical pressure could accelerate whisker growth rates dramatically. They proposed that Sn atoms migrate from the region of high compressive stress to the whisker base along the path of the stress gradient. Since then, others have used mechanically applied stress to induce whisker growth [27–36]. These include application of mechanical stress using indentation [28,30], bending [29,32,35] and in-situ nanoindentation techniques [34,36]. However, the experimentally measured whisker growth rates reported in different studies were drastically different, with some showing

* Corresponding author.
E-mail address: piyush_jagtap@brown.edu (P. Jagtap).

https://doi.org/10.1016/j.scriptamat.2020.02.036
1359-6462/

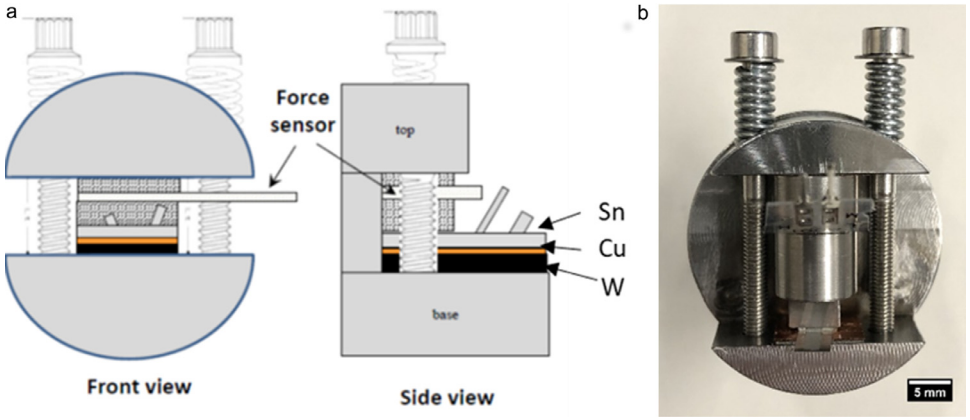

Fig. 1. (a) Schematic drawing of the apparatus for applying pressure on the Sn samples. (b) picture of the actual setup. The apparatus is small enough to fit inside regular SEM chamber.

linear growth kinetics [13,31], some showing non-linear [27,28,30] and others showing limited amounts of growth [34,36]. This may be due to the fact that a constant stress was not maintained on the samples for long durations. Also, some of the previous studies were performed on Sn deposited on reactive substrates making it difficult to relate whisker growth kinetics to the applied stress alone [29,34–36].

In order to overcome the variability in previous studies, the work described here relies on the mechanical application of pressure on the Sn samples. Using a miniaturized test fixture that fits inside an SEM chamber, whisker nucleation and growth kinetics can be studied in real time while a constant pressure is applied to the sample. The results provide measurements that can be compared directly with calculations of the corresponding stress evolution.

The samples consisted of 4 μm Sn layers formed by electrodeposition using stannous sulfate acidic electrolyte [39]. Sn coatings fabricated using stannous sulfate bath are generally more prone to whisker formation compared to commercial methanesulfonic acid (MSA) based baths. Prior to Sn deposition the W substrates were prepared by acid cleaning using a solution of HNO_3, H_2SO_4 and H_2O in 5:3:2 proportion [40], then rinsed in DI water and sonicated to remove any leftover surface residue. A 20 nm Ti layer was then electron-beam evaporated on the W substrate to facilitate adhesion, followed by a 40 nm Cu layer to produce the same crystallographic texture and microstructure as Sn coatings on bulk Cu. After electrodeposition, the Sn samples were allowed to age under ambient conditions for 48 h so that stress induced by IMC formation could saturate. It is worth mentioning that the 40 nm Cu layer did not induce sufficient compressive stress in the Sn layer to initiate whisker formation.

The Sn coated samples were then mounted on the clamping fixture shown in Fig. 1. The fixture was made from stainless steel with the dimensions of SEM specimen mounts so it could be easily transferred in and out of the SEM chamber for periodic observations. The bottom part of the fixture, on which the Sn coated sample is mounted, is rigid whereas the upper part of the fixture is free to move along parallel rails. A flat punch on the bottom of the moveable part applies pressure by tightening the screws on either side of it (see Fig.1). A pair of compression springs mounted around the screws keeps the applied pressure constant over time. A thin film force sensor[1] (Flexiforce® Tekscan) is integrated in the loading axis to monitor the applied force values. The dynamic range of the force sensor used in this study was 0-100 lbs (0-445N).

Direct contact of the punch on the sample made the applied stress non-uniform because of the surface roughness of the Sn layer; higher grains were observed to be flattened whereas adjacent lower grains were untouched. Whiskers were even observed to grow from some of the deformed grains underneath the punch. To apply more uniform pressure, a rectangular piece of steel plate was attached on the sample surface using superglue®, a cyanoacrylate adhesive. Superglue effectively filled the gaps on the Sn surface and formed a very thin skin between Sn and steel plate. The punch was placed on top of the steel plate to apply a uniform pressure on Sn sample. After the screws were tightened and the force was quantified, the clamping system was immediately transferred into the SEM chamber to image the surface. The same regions of the surface were re-imaged periodically over a number of days to observe whisker nucleation and growth in real time. In-between the measurements the sample was stored in ambient atmosphere without removing the load.

A series of SEM micrographs of the same region after varying periods of time under an applied stress of 25 MPa are shown in Fig. 2. Following a short incubation time, nuclei were observed to emerge from the surface of Sn in the vicinity of pressurized edge (shown by white arrows in image). A nucleus is defined as a surface protrusion that has a volume greater than 0.4 um^3. With time, the density of nuclei was found to spread over a distance up to 200 μm away from the pressurized edge. It can be readily seen from Fig. 2 that the nuclei density is higher than the whisker density i.e., not all nuclei that formed after applying pressure eventually formed into longer whiskers. Approximately 25% of the total nuclei eventually grew to become long whiskers and a slightly smaller fraction grew as hillocks.

The stress in the Sn film varies with position and time in the region near the punch. Hence, the nuclei density was measured as a function of position at different time intervals. The density was calculated by counting the number of nuclei in eight adjacent strips of width 10 μm at increasing distance from the pressurized edge. In order to get a statistically reliable value, the density was analyzed from 12 different regions, each 140 × 80 μm, that covered the entire width (~1.7 mm) of the Sn sample. The background was removed using image analysis software to identify the nuclei. An example of counting the nuclei density in a single frame is illustrated in Fig. 3a.

The number density of nuclei vs. distance from the pressurized edge is shown in Fig. 3b for different time periods. The rate of nucleation was rapid in the beginning and slowed down as the time progressed. The width of the distribution can also be seen

[1] The resistance of the sensing material changes when the load is applied. The sensor was caliberated for different applied loads prior to integration in the system. The data was collected utilizing an op amp circuit and an Arduino microcontroller.

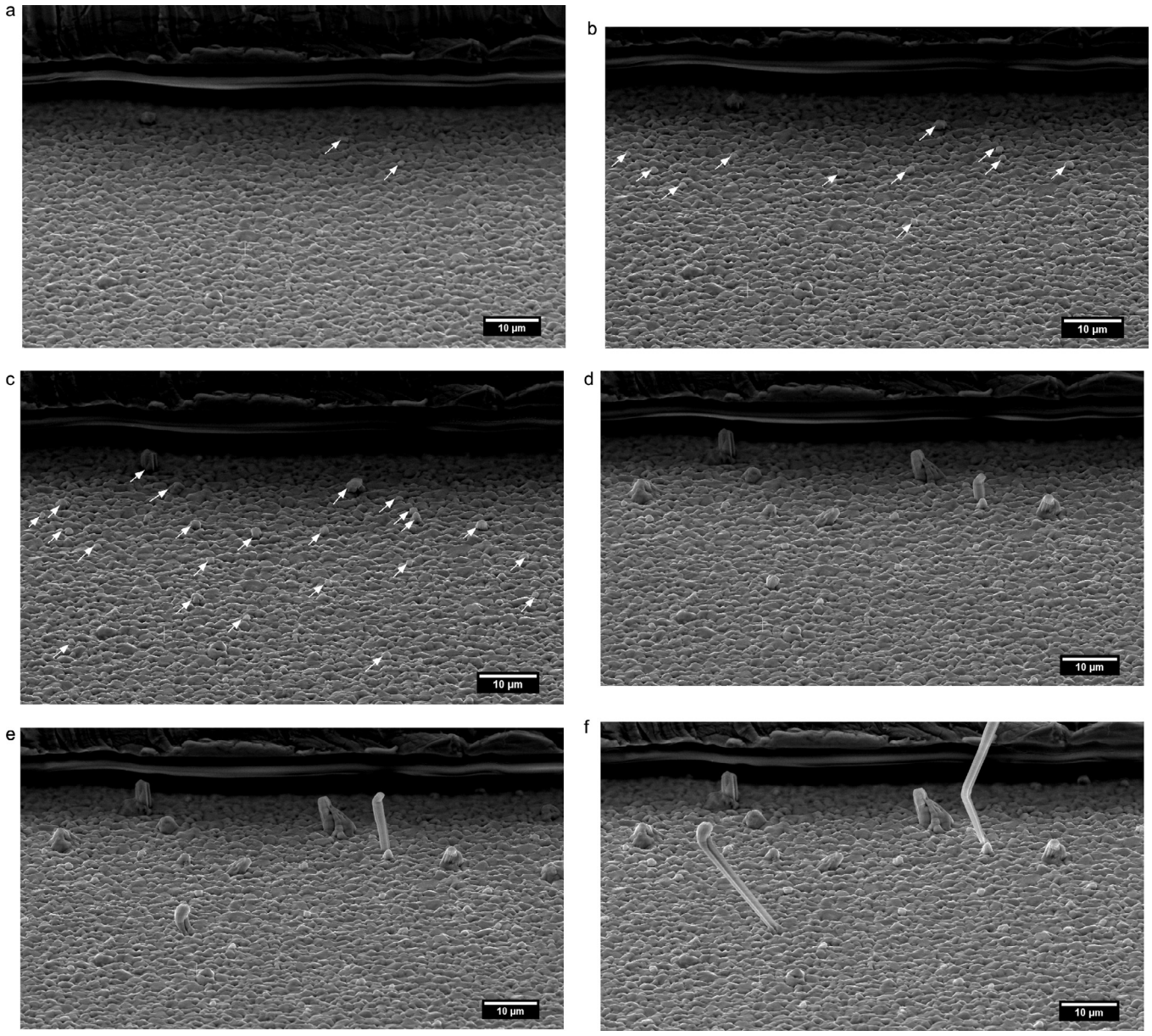

Fig. 2. SEM micrographs of the same region showing whisker nucleation and growth captured in real time after (a) 15 min (b) 1.5 h (c) 6 h (d) 48 h (e) 96 h (f) 267 h. The white arrows in (b) and (c) indicate formation of new whisker nuclei.

to increase as a function of time. The evolution of the width is illustrated in Fig. 3c by plotting the position at which the density reaches a value of 400/mm^2 as a function of time. The position increases more slowly at longer times, consistent with a process that is controlled by diffusive flow.

Previous work using thermally-induced stress [22] suggests that nucleation occurs when the stress exceeds a threshold value (which was 15 MPa). The nucleation kinetics shown here are consistent with this picture in which the stress spreads into the region away from the punch, controlled by the relaxation processes in the layer (diffusion, power-law creep and whisker growth).

In addition to the nucleation density, the growth rate of whiskers was determined from the SEM micrographs. The evolution of a typical whisker is shown in Fig. 4a. To obtain the volume, the whiskers were assumed to have a cylindrical shape and the length and radius were corrected for the angle of growth by comparing measurements made at two different azimuthal angles. The time evolution of multiple whiskers measured within the range of 0–10 microns from the punch is shown in Fig. 4b. All the whiskers observed showed a period of roughly linear growth kinetics after which the growth stopped. The growth rates in the linear regime ranged from 0.5–1.5 µm/day which correlates well with previously reported whisker growth rates [19,41]. It is not clear from these measurements why the individual whiskers stop growing. Possible reasons are that the driving force is depleted in that region or that the microstructure at the base of the whisker changes. This needs to be addressed in future studies, for instance by cross-sectioning the sample to compare the microstructure around whiskers that continue to grow and those that stop (or never grow beyond nuclei).

The average volume of whiskers vs. time was calculated from multiple measurements in each 10 µm interval of distance from the pressurized edge (shown in Fig.4c). The error bars were determined from the standard deviation of the measurements of

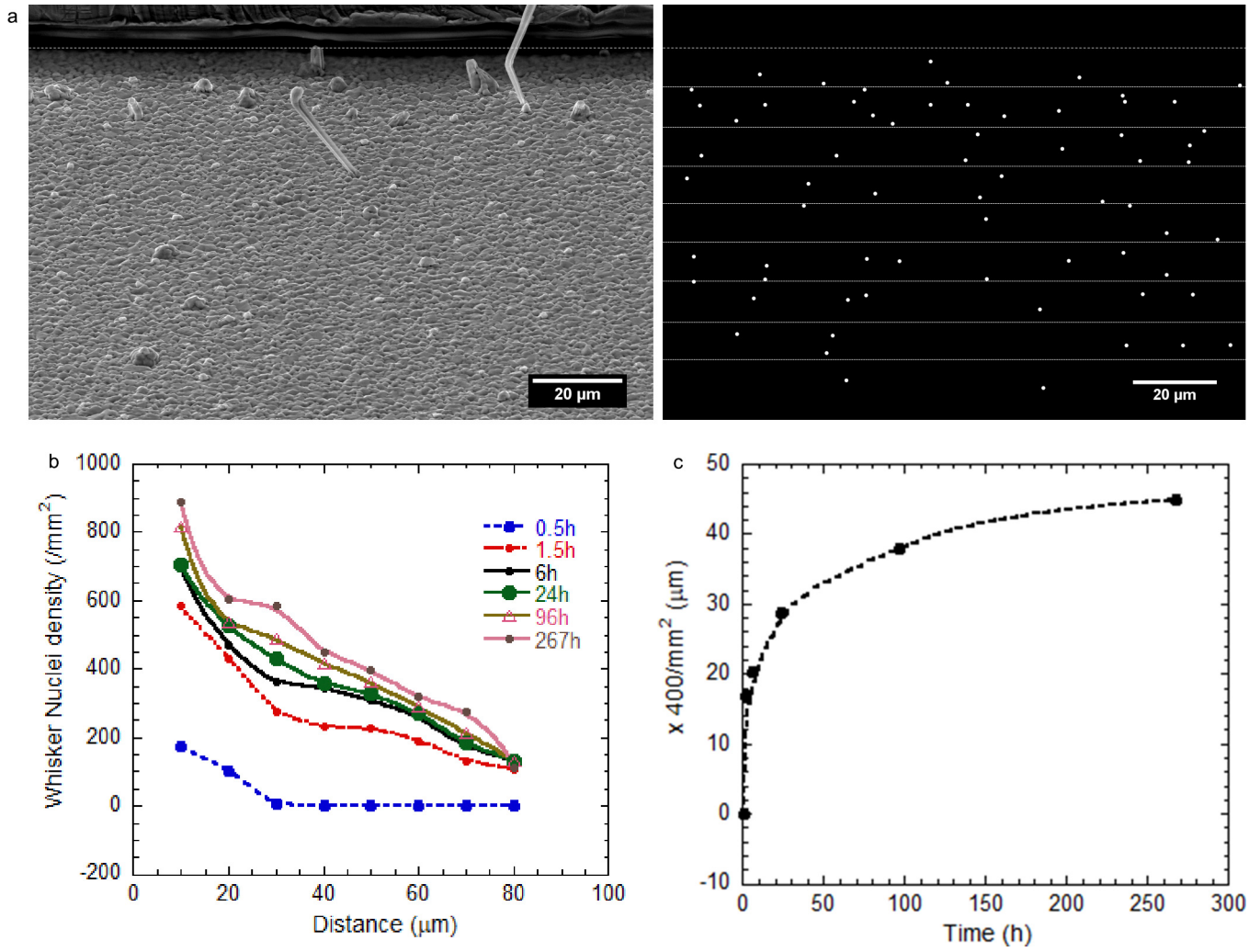

Fig. 3. (a) An illustration of scheme used to calculate nuclei density. (b) Nuclei density away from pressurized edge (c) distance at which nuclei density reaches 400/mm^2 as a function of time.

multiple whiskers. Even though nuclei were observed at further distances, whiskers were only observed to grow within a distance of 30 µm from the pressurized edge over the period of 14 days. On average, whiskers that are farther from the pressurized edge started to grow at a later time and with a slower rate than those closer to the edge. This is similar to the kinetics of nucleation and consistent with the stress spreading away from the deformed region with time. For distances that are further away, the stress (and hence growth rate) takes longer to build-up and has lower values. To correlate the nucleation and growth kinetics with the stress, calculations of the time-dependent stress distribution using finite element analysis (FEA) are planned for future work.

In summary, we report quantitative measurements of whisker nucleation and growth kinetics in real-time inside Scanning Electron microscope under a constant applied stress maintained over a long period of time. The results suggest that both nucleation and growth of whiskers are driven by stress and stress gradients in the Sn layer. As time evolves, the stress spreads out into the Sn layer which induces nucleation and growth further from the region where the pressure is applied. Interestingly, a large fraction of the surface features that nucleate do not continue to grow into whiskers. Because the method allows the time evolution to be observed at different distances form the applied stress, it provides results that can be compared directly with FEA calculations of the stress distribution. Simulating these results with FEA will enable us to determine the kinetic parameters that control whisker growth.

Declaration of Competing Interest

The authors declare that they have no known competing financial interests or personal relationships that could have appeared to influence the work reported in this paper.

Acknowledgement

The authors gratefully acknowledge the support of the NSF-DMR under Contracts DMR-1501411 and DMR-1903071. Authors also acknowledge Prof. Allan Bower for many fruitful discussions on modeling whisker growth and constructive suggestions throughout this work.

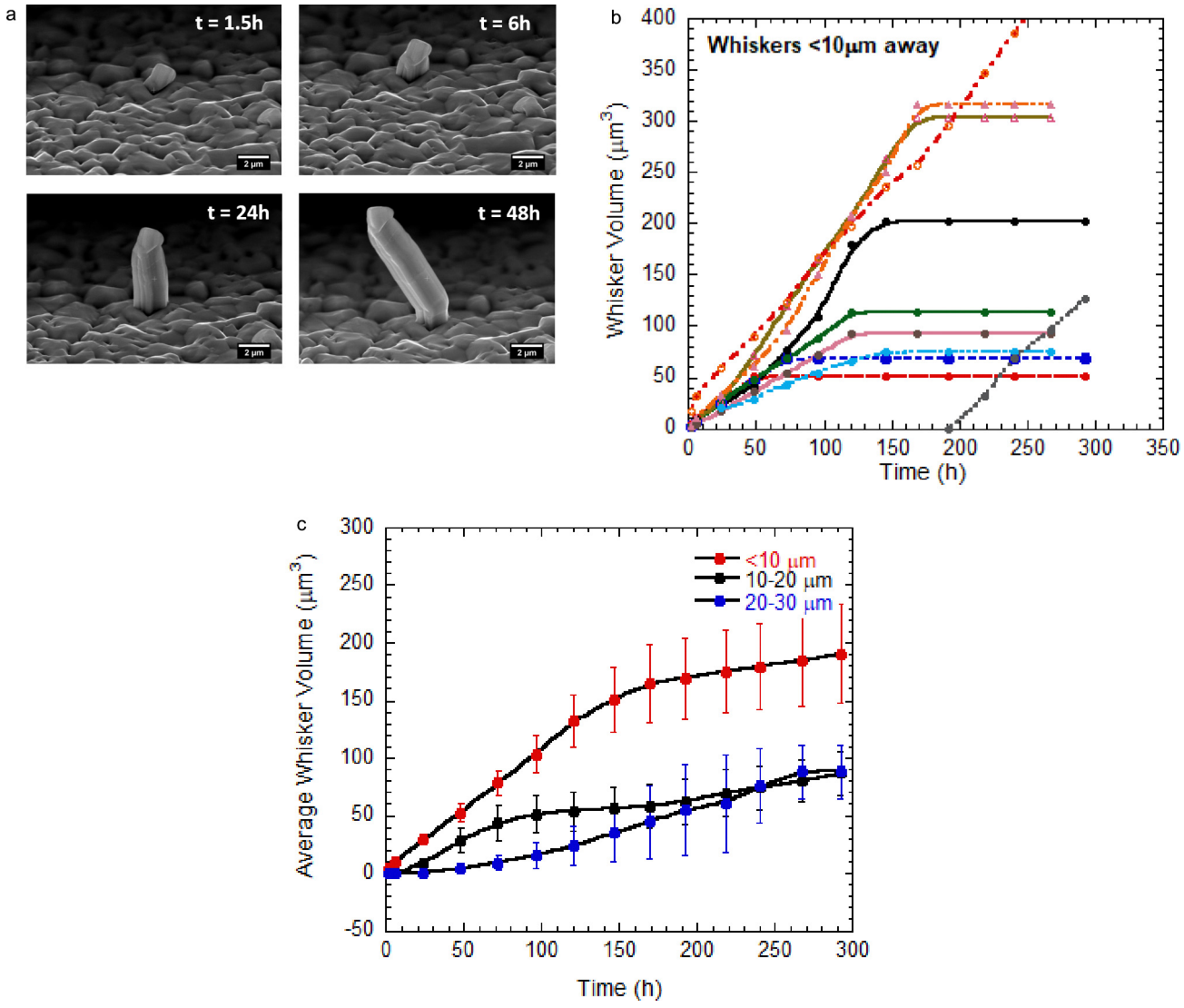

Fig. 4. (a) The time evolution of a typical whisker. (b) the volume of multiple whiskers in the range 0–10 μm (c) average whisker volume at different intervals of distance from the punch.

References

[1] G.T. Galyon, IEEE Trans. Electron. Packag. Manuf. 25 (2005) 94.
[2] S.M. Arnold, Plating 53 (1966) 96–99.
[3] J. Franks, Nature 177 (1956) 984.
[4] F.C. Frank, Phil. Mag. XLIV (1953) 854–860.
[5] J.D. Eshelby, Phys. Rev. 91 (1953) 755–756.
[6] S. Amelinckx, W. Bontinck, W. Dekeyser, F. Seitz, Phil. Mag. 2 (1957) 355–377.
[7] U. Lindborg, Acta Metallurgica 24 (1976) 181–186.
[8] W.C. Ellis, D.F. Gibbons, R.C. Treuting, Wiley, New York, NY, 1958, pp. 102–120.
[9] P.T. Vianco, J.A. Rejent, J. Electron. Mater. 38 (2009) 1815–1825.
[10] P.T. Vianco, J.A. Rejent, J. Electron. Mater. 38 (2009) 1826–1837.
[11] E. Buchovecky, Du N, A. Bower, J. Appl. Phy. 94 (2009) 191904.
[12] K.N. Tu, Phy. Rev. B 49 (1994) 2030.
[13] M. Fisher, L.S. Darken, K.G. Carroll, Acta Metall 2 (1954) 368.
[14] B.Z. Lee, D.N. Lee, Acta Mater 46 (1998) 3701.
[15] W.J. Boettinger, C.E. Johnson, L.A. Bendersky, K.W. Moon, M.E. Williams, G.R. Stafford, Acta Mater 53 (2005) 5033–5050.
[16] E. Chason, N. Jadhav, W.L. Chan, L. Reinbold, K.S. Kumar, Appl. Phy. Lett. 92 (2008) 171901–171903.
[17] M.E. Williams, K.W. Moon, W.J. Boettinger, D. Josell, A.D. Deal, J. Electron. Mater. 36 (2007) 214–219.
[18] K.N. Tu, R.D. Thompson, Acta Metallurgica 30 (1982) 947–952.
[19] K.N. Tu, J.C.M. Li, Mater. Sci. Eng. 409 (2005) 131–139.
[20] J.W. Osenbach, J.M. DeLucca, B.D. Potteiger, A. Amin, R.L. Shook, F.A. Baiocchi, IEEE Trans. Electron. Packag. Manuf. 30 (2007) 23–35.
[21] M.W. Barsoum, E.N. Hoffman, R.D. Doherty, S. Gupta, A. Zavaliangos, Phy. Rev. Lett. 93 (2004) 206104.
[22] F. Pei, C.L. Briant, H. Kesari, A.F. Bower, E. Chason, Scripta Materialia 93 (2014) 16–19.
[23] F. Pei, A.F. Bower, E. Chason, J. Electron. Mater. 45 (2016) 21–29.
[24] F. Pei, E. Buchovecky, A. Bower, E. Chason, Acta Mater 129 (2017) 462–473.
[25] P. Sarobol, J.P. Koppes, W.H. Chen, P. Su, J.E. Blendell, C.A. Handwerker, Mater. Let. 99 (2013) 76–80.
[26] A. Chakraborty, P. Eisenlohr, J. Appl. Phy. 124 (2018) 025302.
[27] C.H. Pitt, R.G. Henning, J. Appl. Phys. 35 (1964) 459.
[28] H. Moriuchi, Y. Tadokoro, M. Sato, T. Furusawa, N. Suzuki, J. Electron. Mater. 36 (2007) 220.
[29] S. Lin, Y. Yorikado, J. Jiang, K. Kim, K. Suganuma, S. Chen, M. Tsujimoto, I. Yanada, J. Mater. Res. 22 (2007) 1975–1986.
[30] T. Shibutani, Q. Yu, M. Shiratori, M.G. Pecht, Microelectron. Reliability 48 (2008) 1033–1039.
[31] H.P. Howard, J. Cheng, P.T. Vianco, J.C.M. Li, Acta Materialia 59 (2011) 1957–1963.
[32] J. Cheng, F. Yang, P.T. Vianco, B. Zhang, J.C.M. Li, J. Electron. Mater. 40 (2011) 2069.
[33] Y. Mizuguchi, Y. Murakami, S. Tomiya, T. Asai, T. Kiga, K. Suganuma, J. Electron. Mater. 41 (2012) 1859–1867.
[34] J.J. Williams, N.C. Chapman, N. Chawla., J. Electron. Mater. 42 (2013) 224.
[35] P. Jagtap, V. Sethuraman, P. Kumar, J. Electron. Mater. 47 (2018) 5229–5242.
[36] I. Lujan-Regalado, A. Kirubanandham, J.J. Williams, N. Chawla, J. Electron. Mater. 48 (2019) 58–71.
[37] E. Chason, N. Jadhav, F. Pei, JOM 63 (2011) 10.
[38] J.W. Shin, E. Chason, J. Mater. Res. 24 (2009) 1522–1528.
[39] P. Jagtap, P. Kumar, J. Electron. Mater. 44 (2015) 1206–1219.
[40] P. Walker, W.H. Tarn, CRC Handbook of Metal Etchants, CRC press, 1990.
[41] E. Chason, N. Jadhav, F. Pei, E. Buchovecky, A. Bower, Prog. Sur. Sci. 88 (2013) 103–131.